catalysts

MDPI

Article

Perovskite-Derivative Ni-Based Catalysts for Hydrogen Production via Steam Reforming of Long-Chain Hydrocarbon Fuel

Kai Guo *,†, Hui Zhang †, Changxuan Zhang, Xining Guo, Huiying Li and Zhourong Xiao *

State Key Laboratory of Metastable Materials Science and Technology (MMST), Hebei Key Laboratory of Applied Chemistry, Yanshan University, Qinhuangdao 066004, China

* Correspondence: kguo@ysu.edu.cn (K.G.); xiaozhourong1234@163.com (Z.X.); Tel./Fax: +86-033-589-2340 (Z.X.)

† These authors contributed equally to this work.

Abstract: Large-scale hydrogen production by the steam reforming of long-chain hydrocarbon fuel is highly desirable for fuel-cell application. In this work, $LaNiO_3$ perovskite materials doped with different rare earth elements (Ce, Pr, Tb and Sm) were prepared by a sol-gel method, and the derivatives supported Ni-based catalysts which were successfully synthesized by hydrogen reduction. The physicochemical properties of the as-prepared catalysts were characterized by powder X-ray diffraction, high-resolution transmission electron microscopy, N_2 adsorption–desorption isotherms, H_2 temperature-programmed reduction, and X-ray photoelectron spectroscopy. The catalytic performance of the as-prepared catalysts for hydrogen production was investigated via the steam reforming of n-dodecane. The results showed that the catalyst forms perovskite oxides after calcination with abundant mesopores and macropores. After reduction, Ni particles were uniformly distributed on perovskite derivatives, and can effectively reduce the particles' sizes by doping with rare earth elements (Ce, Pr, Tb and Sm). Compared with the un-doped catalyst, the activity and hydrogen-production rate of the catalysts are greatly improved with rare earth element (Ce, Pr, Tb and Sm)-doped catalysts, as well as the anti-carbon deposition performance. This is due to the strong interaction between the uniformly distributed Ni particles and the support, as well as the abundant oxygen defects on the catalyst surface.

Keywords: hydrocarbon fuels; steam reforming; hydrogen production; Ni-based catalyst; carbon deposition; $LaNiO_3$ perovskite

Citation: Guo, K.; Zhang, H.; Zhang, C.; Guo, X.; Li, H.; Xiao, Z. Perovskite-Derivative Ni-Based Catalysts for Hydrogen Production via Steam Reforming of Long-Chain Hydrocarbon Fuel. *Catalysts* **2024**, *14*, 186. https://doi.org/10.3390/catal14030186

Academic Editor: Luisa Maria Gomez-Sainero

Received: 21 February 2024
Revised: 4 March 2024
Accepted: 7 March 2024
Published: 8 March 2024

1. Introduction

A fuel cell is a device that converts the chemical energy of hydrogen fuel into electrical energy, which has the characteristics of no combustion or Carnot cycles, a high energy conversion efficiency, low noise levels and zero emission [1,2]. It is regarded as a clean and efficient energy source for the 21st century. Therefore, the development of hydrogen energy has attracted great attention from researchers from all over the world, among which, hydrogen production via the steam reforming of fuel is a very practical method [3]. About 70% of the hydrogen in industry comes from hydrogen production via methane steam reforming [4]. Because methane is a gas at atmospheric pressure, and its transportation and compression costs are relatively high, hydrogen production via methane steam reforming is not suitable for distributed or mobile small-scale automobiles and ships. Therefore, hydrogen production via methane steam reforming technology is more suitable for hydrogen production in fixed areas with large methane reserves, and is not suitable for field and mobile hydrogen production. Diesel and kerosene (long-chain hydrocarbon fuels) have high hydrogen contents per unit volume and are present in the form of a liquid, which is convenient for transportation and storage [5–7]. So, the reforming hydrogen-production technology of liquid fuels such as diesel and kerosene are particularly suitable for hydrogen

production in outdoor automobiles, ships and military submarines [8]. The development of hydrogen production technology for the steam reforming of liquid hydrocarbon fuels has significant implications for both mobile civilian and military equipment [9].

The steam-reforming process of liquid hydrocarbon fuels is relatively complex [10], with the main reaction being the reaction of fuel hydrocarbon molecules with steam, as shown in Equation (1), to form CO and H_2. In addition, there are also water–gas shift reactions (such as Equation (2)) and some reactions of carbon deposition (Equations (3)–(5)).

$$C_nH_{2n+2} + nH_2O = nCO + (2n+1)H_2 \quad (1)$$

$$CO + H_2O = CO_2 + H_2 \quad (2)$$

$$C_nH_m \rightarrow C_2H_4/C_3H_6 \rightarrow C \quad (3)$$

$$CH_4 \rightarrow 2H_2 + C \quad (4)$$

$$2CO \rightarrow CO_2 + C \quad (5)$$

At present, the development of highly active and stable catalysts to improve the efficiency of hydrogen production while inhibiting carbon deposition is the key to achieving this process [11,12]. Among them, noble metal-based catalysts such as Ru, Pt and Rh have attracted the attention of scientists due to their high activity and stability [13–19]. However, because the relative scarcity and high prices of noble metals, large-scale use will inevitably increase costs. Therefore, the development of non-noble metal-based catalysts for fuel steam reforming has received increasing attention in recent years [20,21]. Ni-based catalysts have become a hot research topic due to their high activity and relatively low operating costs [22]. But, the biggest drawback of Ni-based catalysts currently is their relatively low selectivity for reforming, which can easily be accompanied by side reactions such as carbon deposition. In addition, due to the relatively low Taman temperature of Ni metal (591 °C), and that the temperature of the reforming reaction is generally higher than its Taman temperature, the active component Ni is prone to sintering and agglomeration, greatly reducing the service life of the catalyst [23–25].

There are various common strategies to improve catalyst stability, such as reducing the acidic sites of the support [26], enhancing metal–support interaction and constructing surface oxygen defects [27,28]. Masanori et al. [29] studied the use of La_2O_3-modified Ni/Al_2O_3 catalysts for kerosene steam reforming and found that the activity, stability and hydrogen yield of the catalysts were increased. This is attributed to the fact that La_2O_3 modification enhances the dispersion of Ni and reduces the acidic sites of the support, thereby reducing carbon deposition. Our group [30–33] studied the use of ceria-modified alumina or silica-supported Ni-Co bimetallic catalysts for the steam reforming of n-dodecane. It was found that ceria modification increased the dispersion of Ni-Co, enhanced the interaction between metal–support, and reduced the acidic sites on the support surface, thereby increasing the activity and stability of the catalyst. In recent years, the activity and stability of catalysts have been greatly improved by regulating the oxygen vacancies and metal–support interactions on the support [34–36]. Owing to the extremely important role of the support in the catalyst system, it can not only promote the dispersion of active components, but also suppress the sintering of active metals when there is a strong interaction between the support and metal. Among them, perovskite (ABO_3) supports are a widely used type of support [37–39]. Its A and B sites can be finely regulated and substituted, and it has very high sintering resistance, showing good application prospects in many fields [40]. More importantly, perovskite oxides have abundant surface oxygen vacancies, which facilitate the activation of reactant water molecules and accelerate the elimination of carbon-deposition intermediates, thus enhancing the activity and anti-carbon-deposition performance of catalysts [41,42]. However, how to finely regulate the metal sites and oxygen-defect sites of perovskites remains a big challenge at present.

Based on this, $LaNiO_3$ perovskite materials doped with different rare earth elements (Ce, Pr, Tb and Sm) were synthesized by the sol-gel method, and perovskite-derivative Ni-

based catalysts were successfully synthesized by hydrogen reduction. The as-prepared catalysts were systematically analyzed and characterized using wide-angle X-ray diffraction, high-resolution transmission electron microscopy, temperature-programmed reduction, N_2 adsorption–desorption, and X-ray transmission photoelectron spectroscopy. A study was conducted on the catalytic hydrogen production via the steam reforming of n-dodecane. The results showed that by controlling the doping of rare earth elements (Ce, Pr, Tb, and Sm), the size of nickel metal nanoparticles and the concentration of oxygen defects on the catalyst surface can be controlled, thereby exhibiting a different conversion of n-dodecane and hydrogen production rates. Moreover, doping with rare earth elements (Ce, Pr, Tb, and Sm) significantly improves the activity and anti-carbon-deposition performance of the catalyst.

2. Experimental Section

2.1. Chemicals and Materials

Nickel nitrate hexahydrate ($Ni(NO_3)_2{\cdot}6H_2O$, Tianjin Guangfu Fine Chemical Research Institute, AR), lanthanum nitrate hexahydrate ($La(NO_3)_3{\cdot}6H_2O$, Tianjin Guangfu Fine Chemical Research Institute, AR), cerium nitrate hexahydrate ($Ce(NO_3)_3{\cdot}6H_2O$), samarium nitrate hexahydrate ($Sm(NO_3)_3{\cdot}6H_2O$), protactinium nitrate hexahydrate ($Pr(NO_3)_3{\cdot}6H_2O$), terbium nitrate hexahydrate ($Tb(NO_3)_3{\cdot}6H_2O$, Huawei Ruike, AR, Beijing, China), dodecane ($C_{12}H_{26}$, Tianjin China Kemio Chemical Reagent Co., Ltd., AR, Tijanjin, China), citric acid (CA) and ethylene glycol (EG) were purchased from Sinopharm Chemical Reagent Co., Ltd., Shanghai, China, as were nitrogen/helium (high-purity, hexagonal gas company) and deionized water.

2.2. Preparation of Catalysts

The catalysts were prepared by sol-gel method [41]. Taking $LaNiO_3$ synthesis as an example, firstly, 4.33 g (10 mmol) $La(NO_3)_3{\cdot}6H_2O$ and 2.91 g (10 mmol) $Ni(NO_3)_2{\cdot}6H_2O$ were added to 100 mL deionized water and stirred evenly at room temperature. Then, we added 4.20 g (20 mmol) of citric acid and 5.0 mL of ethylene glycol and stirred for 4 h until the mixture was uniform. We transferred the mixed solution to a heater and heated it at a heating temperature of 120 °C. The aqueous solution was removed by evaporation to obtain gel. We transferred the obtained gel to an oven for drying for 12 h at a temperature of 120 °C. After drying, a solid substance was obtained. The solid substance was ground into a solid powder with a mortar, and then calcined at a muffle furnace with 800 °C for 3 h to obtain $LaNiO_3$. Then, we placed the calcined $LaNiO_3$ in an atmosphere furnace, and reduced it at 650 °C under a 5% Vol H_2/Ar mixture for 1 h to prepare the reduced catalyst. Catalysts doped with different rare earth elements were synthesized by using the same method, where the atomic ratio of La:Ce:Ni in $LaCeNiO_3$ was 0.8:0.2:1, the atomic ratio of La:Ce:Pr:Ni in $LaCePrNiO_3$ was 0.8:0.1:0.1:1, the atomic ratio of La:Ce:Sm:Ni in $LaCeSmNiO_3$ was 0.8:0.1:0.1:1 and the atomic ratio of La:Ce:Tb:Ni in $LaCeTbNiO_3$ was 0.8:0.1:0.1:1.

2.3. Characterization

The phase of structure analysis for the prepared catalyst, precursor and reduced catalyst was carried out using Rigaku D8-Focus X-ray diffractometer from Nippon Institute of Science Saitama, Japan. The testing conditions for a wide-angle X-ray diffractometer are Cu target, K α Ray (λ = 0.154 nm), tube voltage of 40 kV, tube current of 200 mA, scanning speed of 8 °/min, and scanning range of 10° to 80°. The morphology and nanoparticles of the catalyst were observed using the Tecnai G2 F20 transmission electron microscopy (TEM) from FEI in Eindhoven, The Netherlands, with an operating voltage of 150–300 kV. The distribution of elements was analyzed using surface scanning. The pore structure of the material was analyzed using Micromeritics Tristar 3000 (Norcross, GA, USA), with parameters of nitrogen atmosphere at −196 °C. Before sample testing, degassing and dehydration were required at 300 °C. Temperature-programmed reduction was tested on

the AMI-300 chemical-adsorption instrument (Tuggerah, Australia). Firstly, we weighed a certain mass of a powder sample and pretreated it in an Ar atmosphere at 400 °C for 1 h. After cooling to 50 °C, a 10% Vol H_2–Ar mixture gas was introduced, and the temperature was raised from 50 °C to 800 °C at a heating rate of 10 °C/min. The carbon deposition of the catalyst after the reaction was characterized using a TQ-500 thermal analyzer (Tokyo, Japan). Approximately 10 mg of the sample was weighed and placed in a ceramic crucible. The temperature was raised from room temperature to 800 °C in an air atmosphere at a heating rate of 10 °C/min to obtain the weight loss curve of the sample. The DTG data can be obtained by first-order differentiation of the weightlessness curve. Raman spectra were measured using a DXR Microscope system (Waltham, MA, USA). The sample (50 mg) was loaded and excited under an argon laser (532 nm).

2.4. Catalytic Performance Evaluation

The hydrogen production via the steam reforming of n-dodecane was carried out in a stainless-steel tubular fixed bed reactor, as shown in Figure S1. Before the reaction, the catalyst was compressed to a pressure of 10 MPa, and then sieved to obtain a catalyst with a mesh size of 20–40. We mixed 0.25 g of catalyst with 1.2 g of quartz sand and filled it evenly in a stainless-steel tube with a diameter of 6 mm. We sealed it, then introduced nitrogen gas and raised the temperature to 650 °C. It reduced for 1 h in a 5% Vol H_2/Ar mixture, then was switched to nitrogen to stabilize the system temperature to reaction temperature (600 °C) at atmospheric pressure. We input a constant amount of water using a high-pressure metering pump and gasified it at 300 °C for 15 min. Then, liquid n-dodecane was introduced, with a feed rate of 15 mL/g_{cat}·h. After gasification at 300 °C and mixing with steam, it was uniformly introduced into the catalyst bed. After the reaction, the product underwent condensation and drying. Then, the composition and content of the gas phase products were analyzed online using portable micro-gas chromatography (Micro GC-490, Agilent, Santa Clara, CA, USA). The detector for chromatography was a TCD detector, equipped with three chromatography columns. Firstly, activated alumina columns were used to detect hydrocarbon molecules of C_3 and above. Secondly, PPU columns were used to detect CO_2, ethane and ethylene. Finally, 5 Å MS columns were used to detect H_2, N_2, CH_4 and CO. We calculated the conversion rate of n-dodecane based on the analysis results of gas-phase products (Equation (6)). We calculated the yield and composition of gas-phase products based on the analysis results (Equations (7) and (8)).

$$X_{12}\ (wt\%) = \frac{F_{CO}^{out} + F_{CO2}^{out} + F_{CH4}^{out}}{12F_{c12}^{in}} \times 100 \quad (6)$$

$$\text{Gas formation rate (mmol/min) } R(H_2) = \frac{A_{H2} \cdot f_{H2}}{A_{N2} \cdot f_{N2}} \times R(N_2) \quad (7)$$

$$V\%(H_2) = \frac{R(H_2)}{\sum R(H_2 + CO + CO_2 + CH_4)} \times 100 \quad (8)$$

In Equation (6), the conversion of X_{12}—n-dodecane, %. R(N_2) = 60 mL/min, F_{C12}^{in}—in total amount of carbon entering the reactor, mmol/min. F_{CO}^{out}, F_{CO2}^{out}, F_{CH4}^{out}—the total number of C_1 products in the product leaving the reactor, mmol/min. In Equation (7), R(N_2) = 60 mL/min, which is the nitrogen flow rate. A_{H2} and f_{H2} represent the chromatographic peak area and response factor of H_2, respectively. A_{N2} and f_{N2} represent the peak area and response factor of N_2 obtained in the chromatography, respectively. In Equation (8), V%(H_2)—the percentage content of hydrogen gas in dry gas (excluding nitrogen).

3. Results and Discussion

3.1. Structural and Morphological Characteristics of Catalysts

The XRD patterns of the catalysts after calcination are shown in Figure 1a. After calcination, the catalysts mainly exist in the crystal structure of $LaNiO_3$ (PDF-34-1181)

perovskite [37]. With the doping of rare earth elements, the diffraction peak intensity of the crystal structure of perovskite significantly decreases, which may be due to the heteroatom doping hindering crystal growth, resulting in a decrease in the crystallinity of perovskite [42]. In addition, the La_2O_3 structure appeared after doping with rare earth elements, and without the structure of doped oxide and nickel oxide alone. This indicates that rare earth elements can partially replace La elements and enter the interior of perovskite crystals and are highly dispersed in perovskite oxides.

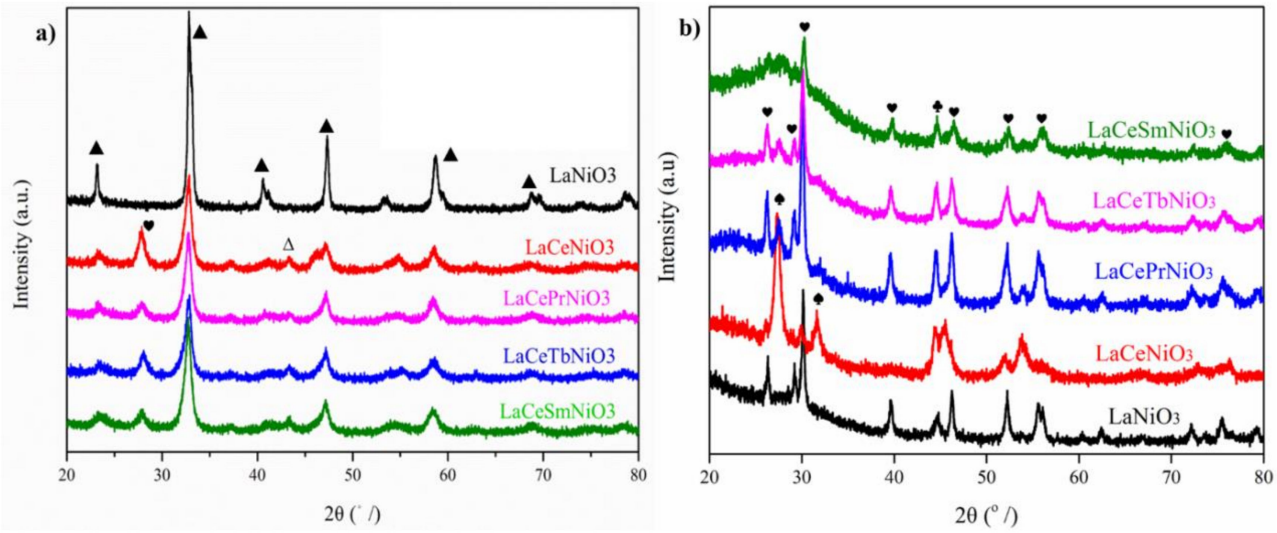

Figure 1. XRD patterns of the catalysts that after calcination (**a**) and (**b**) catalysts after hydrogen reduction. The symbol of Δ, ♥, ▲, ♠ and ♣ represented NiO, La_2O_3, $LaNiO_3$ perovskite, CeO_2 and Ni, respectively.

The XRD patterns of the reduced catalysts are shown in Figure 1b. Due to the reduction temperature of 650 °C, perovskite is easily reduced to Ni metal and La_2O_3 [37]. Therefore, new diffraction peaks dominated by La_2O_3 appeared in the reduced catalysts, and a characteristic peak of Ni metal appeared at 44.5 °C [43]. For $LaCeNiO_3$ catalyst, in addition to Ni and La_2O_3, there are also characteristic peaks of CeO_2. The CeO_2 peak that appeared after reduction only for the $LaCeNiO_3$ catalyst may be attributed to the content of Ce in $LaCeNiO_3$ being higher than that of other catalysts. The above results indicate that perovskite is transformed into oxide after reduction, which can effectively load Ni metal.

The TEM results showed that the surface of the reduced perovskite-derived material is rich in nickel nanoparticles, and some pores can be observed (Figures 2a,d and S2a). HRTEM showed that the lattice spacing of nickel nanoparticles was 0.20 nm, and La_2O_3 with a lattice spacing of 0.29 nm was observed (Figures 2b,e and S2b,d), indicating that $LaNiO_3$ perovskite was transformed into Ni metal and La_2O_3 after hydrogen reduction [44]. In addition, elemental surface mapping showed that particles size of nickel is approximately 25 nm (Figure 2c). After doping with rare earth elements Ce (Figure S2e) and Pr (Figure S2f), the particle size of nickel decreases to 20 nm (Figure 2f), indicating that rare earth doping can reduce the particle size of nickel [45]. The above results suggested that perovskite-derivative Ni-based catalysts can be successfully constructed.

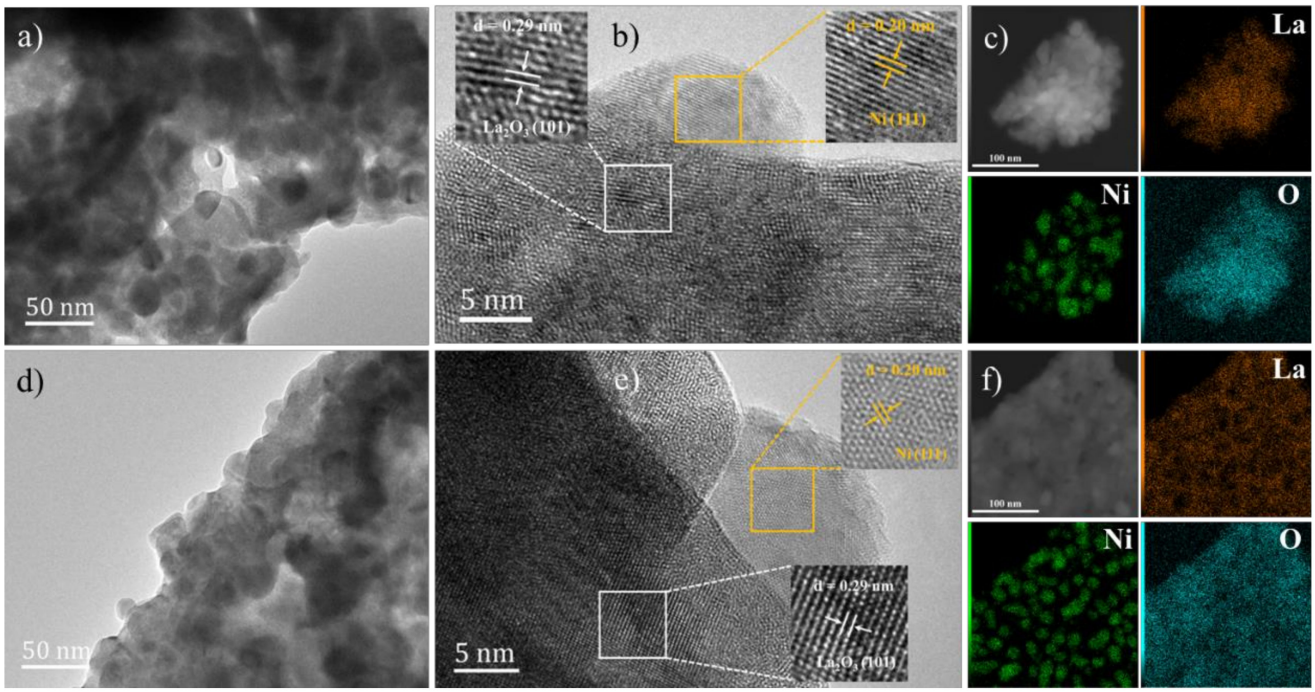

Figure 2. (**a**) TEM images and (**b**) HRTEM images of $LaNiO_3$, (**c**) the element mapping of $LaNiO_3$ after hydrogen reduction. (**d**) TEM images and (**e**) HRTEM images of $LaCePrNiO_3$, (**f**) the element mapping of $LaCePrNiO_3$ after hydrogen reduction.

The N_2 adsorption–desorption isotherms of the catalysts after calcination are shown in Figure 3a. The hysteresis loop of the adsorption–desorption isotherms can be clearly observed from Figure 3a, indicating that the as-prepared catalysts are mesoporous materials. In addition, as the relative pressure increases, the adsorption capacity also increases, indicating the presence of a certain amount of macropores [46]. The pore-size distribution curve is shown in Figure 3b, and the prepared materials exhibit a dual pore-size distribution. Among them, the mesoporous pore size is around 36 nm, and the macroporous pore size is around 60 nm. The specific surface area, pore volume and pore size data of the catalysts after calcination are summarized in Table 1. In Table 1, the specific surface area of the catalysts is relatively small, and the pore size is relatively large, with an average pore size of 14–23 nm.

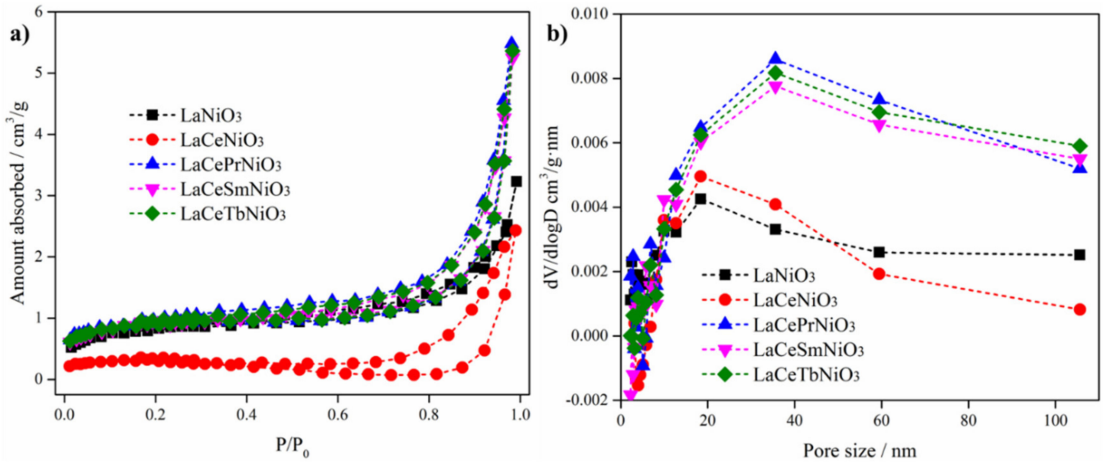

Figure 3. (**a**) N_2 adsorption–desorption isotherms and (**b**) pore size distributions of the as-prepared sample.

Table 1. The textural properties of as-prepared sample.

Sample	BET Surface Area (m^2/g)	Pore Volume (cm^3/g)	Average Pore Size (nm)
$LaNiO_3$	2.84	0.65	14.29
$LaCeNiO_3$	1.15	0.26	13.00
$LaCePrNiO_3$	3.30	0.76	17.59
$LaCeSmNiO_3$	3.28	0.75	23.84
$LaCeTbNiO_3$	3.02	0.75	20.69

The H_2 temperature-programmed reduction of the catalysts is shown in Figure 4. There are three reduction peaks distributed in the low temperature, medium temperature and high temperature regions (Figure 4). The reduction peaks belong to the reduction of surface oxygen, $LaNiO_3$ to $LaNiO_{2.5}$, and $LaNiO_{2.5}$ to Ni metal, respectively [43,44]. The shoulder peak between 300 and 350 °C belongs to the reduction of surface oxygen, as confirmed by previous work [39]. The peak intensity increases with rare earth-element doping, suggesting increased surface oxygen vacancy. It was found that after doping with rare earth elements, the reduction temperature of the catalysts shifted towards the high-temperature region, indicating an enhanced interaction strength between NiO and the support. The two main reduction peaks of $LaNiO_3$ are at 350 °C and 500 °C. After doping with rare earth elements, these two reduction peaks both shift towards the high-temperature region. The two main reduction peaks of $LaCePrNiO_3$ are concentrated at temperatures of 425 °C and 513 °C, and the peak areas in the high-temperature region are relatively large, indicating that the catalyst has stronger metal–support interactions. Previous research has shown that stronger metal–support interactions contribute to the dispersion and sintering resistance of reduced metals [47,48]. As a result, the catalyst may exhibit good activity, stability and anti-carbon deposition.

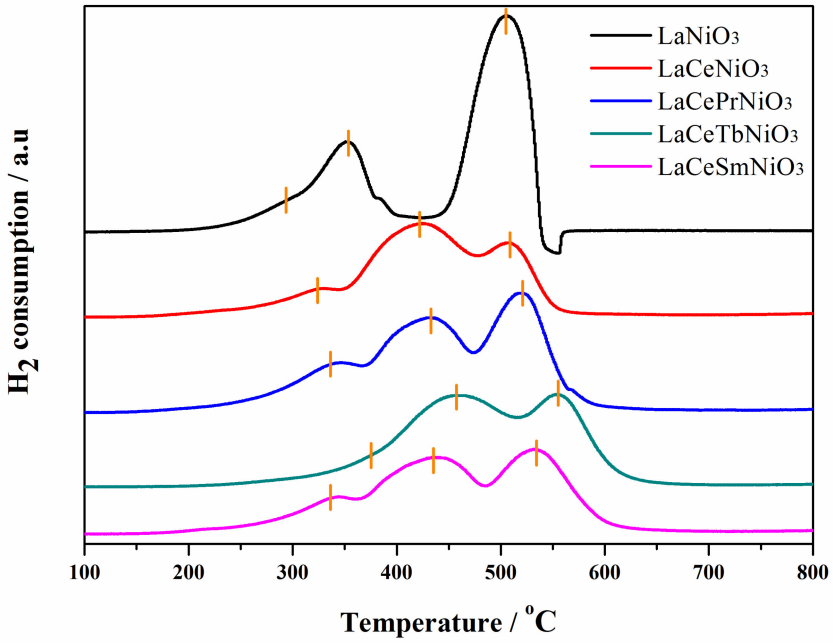

Figure 4. H_2-TPR profiles of the as-prepared catalysts.

Figure 5 shows the XPS spectra of La 3d in the samples. The peaks of 835 eV, 838.55 eV and 852.03 eV, 855.39 eV correspond to La $3d_{5/2}$ and La $3d_{3/2}$ in $LaNiO_3$, respectively (Table 2). After doping with rare earth elements, the electron-binding energy of La shifts towards the direction of low binding energy, indicating that La has obtained electrons. The Ce-3d and Pr-3d are showed in Figure S3a and S3b, respectively. Four peaks can be observed in the O 1s spectra of $LaNiO_3$, $LaCeNiO_3$ and $LaCePrNiO_3$ (Figure 5). They belong

to lattice oxygen (O_L), oxygen vacancies (O_V), surface oxygen (O_{surf}), and adventitious oxygen (O_{adv}), respectively [42]. According to XPS peak-fitting calculations, the proportion of lattice oxygen in the sample has increased. However, the catalyst surface is mainly composed of oxygen vacancies, surface oxygen, and adventitious oxygen, accounting for more than 75.2% (Table 3). In addition, the XPS results of Ni 2p were observed. The three peaks at 852 eV, 855.5 eV and 865 eV belong to Ni^0, Ni^{2+} and satellite peaks (Ni^{2+}), respectively. The binding energies of Ni^0 in $LaNiO_3$, $LaCeNiO_3$ and $LaCePrNiO_3$ are 852 eV, 852.1 eV and 852.16 eV, indicating that the electron-binding energy of Ni^0 in the catalysts doped with rare earth elements shifts towards lower binding energies. This indicates that the increase in electron density of Ni^0 may be explained by the enhanced strength of the metal–support interaction, which is consistent with the results of H_2-TPR. Moreover, previous studies have indicated that the electron density of nickel enhances the activation and dissociation of C–H bonds [49]. The ratio of $Ni^0/(Ni^0 + Ni^{2+})$ was also calculated, and the Ni^0 ratios for $LaNiO_3$, $LaCeNiO_3$ and $LaCePrNiO_3$ were about 54.1%, 55.6% and 56.8%, respectively. This result suggests that the proportion of nickel metal in the three catalysts is similar, excluding the influence of different nickel metal contents on catalytic performance.

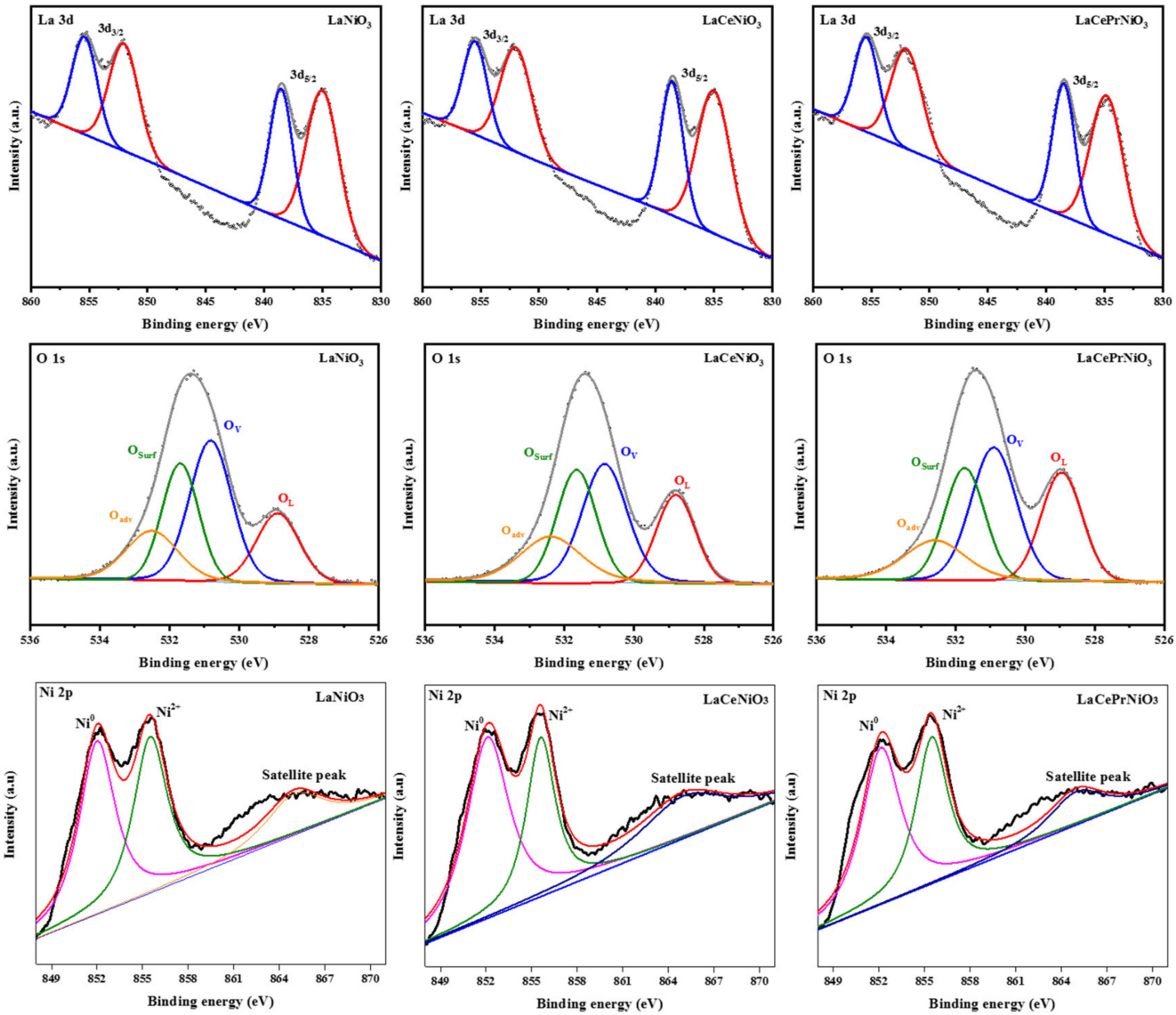

Figure 5. XPS spectra of the catalysts after reduction.

Table 2. XPS of La 3d for $LaNiO_3$, $LaCeNiO_3$ and $LaCePrNiO_3$.

Sample	Name	Peak Position (eV)	Area	Percentages (%)
$LaNiO_3$	La $3d_{5/2}$	835	89,853.57	35.4
		838.55	56,589.05	22.3
	La $3d_{3/2}$	852.03	60,555.37	23.8
		855.39	46,967.88	18.5
$LaCeNiO_3$	La $3d_{5/2}$	835	60,051.57	35.8
		838.59	37,870.52	22.6
	La $3d_{3/2}$	851.97	41,413.96	24.6
		855.47	28,454.67	17.0
$LaCePrNiO_3$	La $3d_{5/2}$	834.83	72,638.22	35.0
		838.49	47,519.36	22.9
	La $3d_{3/2}$	851.99	49,820.91	24.0
		855.41	37,590.91	18.1

Table 3. XPS of O 1s for $LaNiO_3$, $LaCeNiO_3$ and $LaCePrNiO_3$.

Sample	Name	Peak Position (eV)	Area	Percentages (%)
$LaNiO_3$	O_L	528.9	13,140.8	19.1
	O_V	530.82	26,106.83	37.9
	O_{Surf}	531.69	17,864.29	25.9
	O_{adv}	532.51	11,747.81	17.1
$LaCeNiO_3$	O_L	528.81	10,728.15	20.0
	O_V	530.85	18,226.5	33.9
	O_{Surf}	531.66	14,346.38	26.7
	O_{adv}	532.4	10,391.31	19.4
$LaCePrNiO_3$	O_L	528.95	16,498.19	24.8
	O_V	530.91	23,063.9	34.8
	O_{Surf}	531.74	16,776.45	25.2
	O_{adv}	532.6	10,121.5	15.2

3.2. Catalytic Performance for H_2 Production

Figure 6 shows the conversion rate and gas production rate of n-dodecane steam reforming catalyzed by the catalysts. As shown in Figure 6a, the initial conversion of n-dodecane on $LaNiO_3$ catalyst was 53.5%, and the yield of hydrogen was 4.99 mmol/min. After 150 min of reaction, the conversion rate of n-dodecane decreased to 43.2%, and the yield of hydrogen was 3.87 mmol/min. The conversion of n-dodecane and the yield of hydrogen decreased by 19.2% and 22.44%, respectively. After the adding of Ce, the stability of the catalysts was significantly improved, with a conversion rate of 51.3% for n-dodecane and a hydrogen yield of 5.35 mmol/min for $LaCeNiO_3$. And, the conversion rates of n-dodecane on $LaCePrNiO_3$, $LaCeTbNiO_3$ and $LaCeSmNiO_3$ catalysts were 70%, 55% and 65% (Figure 6f), respectively. Especially for the $LaCePrNiO_3$ catalyst, the conversion was as high as 70%, and the yield of hydrogen reached 5.9 mmol/min. After 300 min of reaction, there was no significant decrease in the conversion and hydrogen-production rate. This result indicates that the activity, stability, and hydrogen-production rate of the catalyst were significantly improved after doping with rare earth elements.

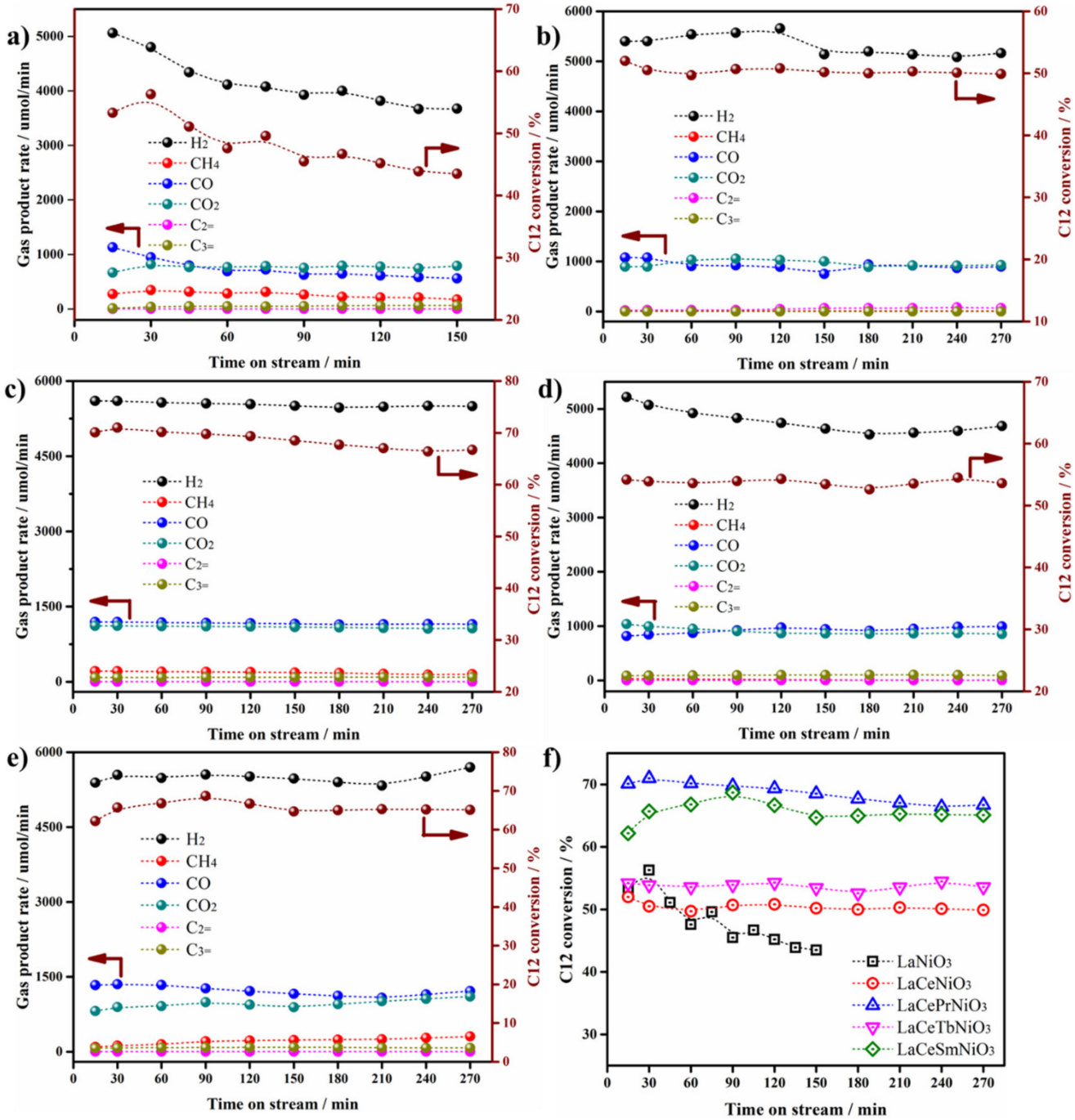

Figure 6. The conversion of n-dodecane and gas product rate for (**a**) $LaNiO_3$, (**b**) $LaCeNiO_3$, (**c**) $LaCePrNiO_3$, (**d**) $LaCeTbNiO_3$, (**e**) $LaCeSmNiO_3$ and (**f**) comparison of the conversion of n-dodecane. Reaction condition: 600 °C, 0.1 MPa, LHSV of $C_{12}H_{26}$ 15 mL/g_{cat}·h, with mole ratio of H_2O:$C_{12}H_{26}$ at 24.

The composition of gas-phase products is shown in Figure 7, where the composition of H_2 in dry gas was about 70%, and the proportion of CO and CO_2 reached about 10–20% [15]. This result is consistent with the previously reported results of hydrogen production via the steam reforming of n-dodecane. The proportion of CO in $LaNiO_3$ gradually decreases, indicating that its catalytic activity is also gradually decreasing, which is consistent with the results in Figure 6a. The catalyst doped with rare earth elements showed almost no significant change in gas-phase composition, indicating the good stability of the catalyst.

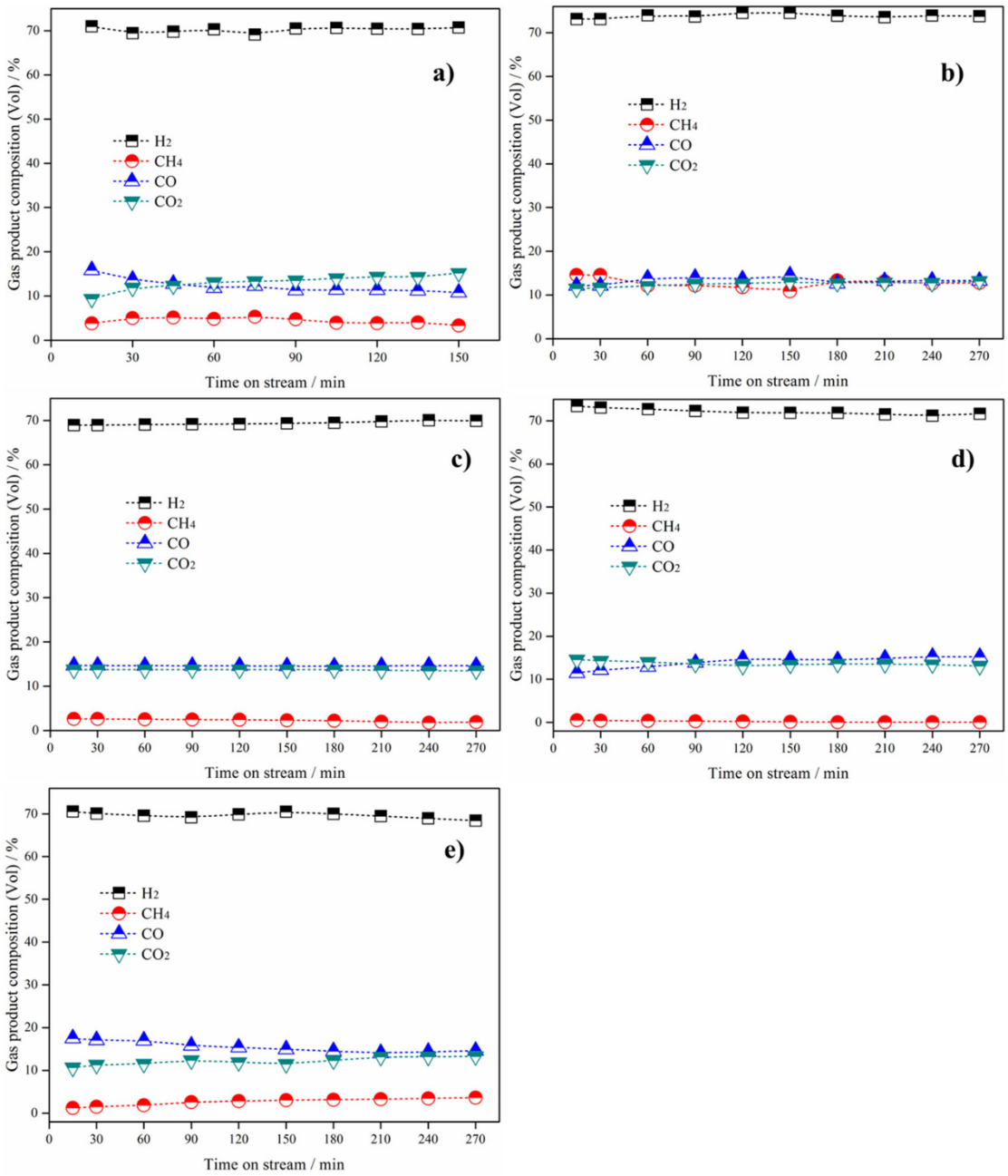

Figure 7. The relative contents of the gas products for steam reforming of n-dodecane. (**a**) $LaNiO_3$, (**b**) $LaCeNiO_3$, (**c**) $LaCePrNiO_3$, (**d**) $LaCeTbNiO_3$ and (**e**) $LaCeSmNiO_3$. Reaction condition: 600 °C, 0.1 MPa, LHSV of $C_{12}H_{26}$ 15 mL/g_{cat}·h, with mole ratio of H_2O:$C_{12}H_{26}$ at 24.

We also tested the performance of the catalysts under the condition of H_2O:$C_{12}H_{26}$ mole ratio of 48, as shown in Figure 8a,b. The initial conversion rate of n-dodecane using the $LaNiO_3$ catalyst was 58%, and the yield of hydrogen gas was 5.1 mmol/min. After 270 min of reaction, the conversion rate increased to 70% and the hydrogen production rate increased to 5.88 mmol/min, indicating that increasing the amount of water in the reaction can greatly improve the conversion, hydrogen production rate and stability. The $LaCePrNiO_3$ catalyst has a conversion rate of up to 88% and a hydrogen gas yield of 6.6 mmol/min. After 300 min of reaction, there was no significant decrease in conversion rate and hydrogen-production rate. This result indicates that the activity, stability and hydrogen-production rate of the catalyst have been significantly improved after doping with rare earth elements.

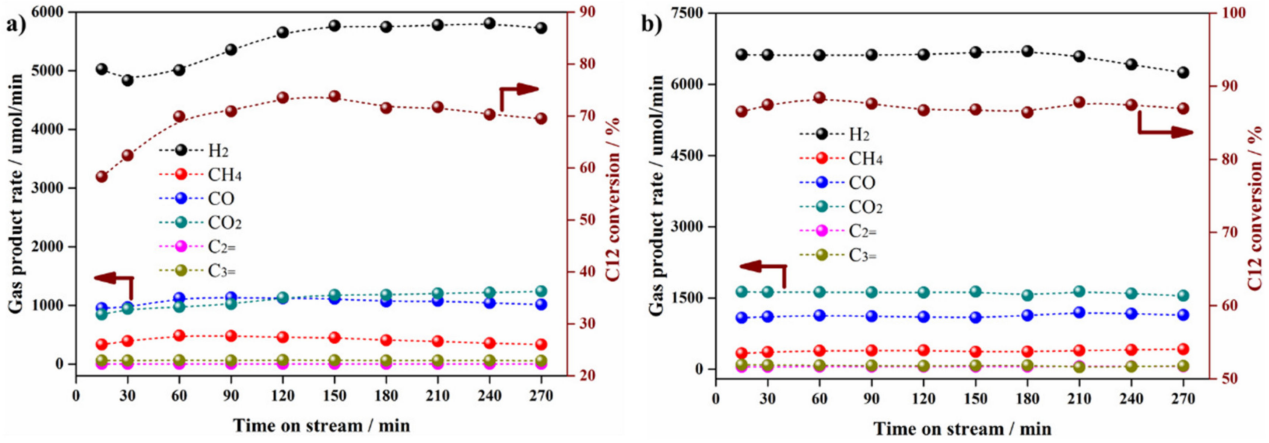

Figure 8. The conversion of n-dodecane and gas-production rate for (**a**) $LaNiO_3$ and (**b**) $LaCePrNiO_3$. Reaction condition: 600 °C, 0.1 MPa, LHSV of $C_{12}H_{26}$ 15 mL/g_{cat}·h, with mole ratio of H_2O:$C_{12}H_{26}$ at 48.

3.3. Analysis of Carbon Deposition on Catalyst after Reaction

The carbon deposition on the surface of the catalysts after the reaction was analyzed by using thermogravimetric techniques, and the results are shown in Figure 9 (solid line). The weight-loss rate of the $LaNiO_3$ catalyst was 33%, indicating the presence of a large amount of carbon deposition on the surface of the catalyst after the reaction [50]. After the introduction of rare earth element Ce, the weight-loss rate of the $LaCeNiO_3$ catalyst was significantly reduced. Its weight-loss rate was 20%, indicating that the introduction of rare earth Ce doping reduces carbon deposition. Further introduction of other rare earth elements reduces the weight-loss rate of the catalyst to a certain extent, indicating a further reduction in carbon deposition. Especially when Ce and Pr were co-doped, the weight-loss rate was only 10%. The above results indicate that the introduction of rare earth dopants significantly reduces the carbon deposition of the catalyst, suggesting a significant improvement in the catalyst's anti-carbon deposition performance. This can be attributed to the points as follows: firstly, the addition of rare earth elements leads to a stronger metal–support interaction, resulting in smaller nanoparticles size of nickel metal. The presence of smaller nickel nanoparticles helps to suppress the formation of carbon deposition. Secondly, the addition of rare earth elements results in abundant oxygen defects on the surface of the catalyst (H_2-TPR and O 1s XPS), which helps to eliminate carbon deposition.

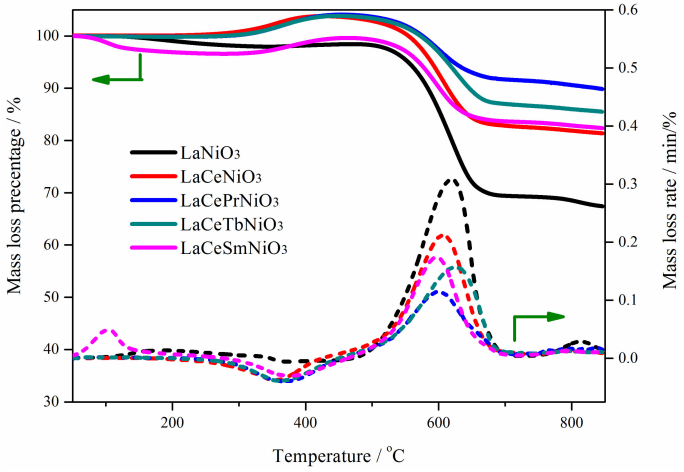

Figure 9. The TG and DTG analysis of the spent catalysts.

The differential thermal analysis of the catalyst after the reaction is shown by the dashed line in Figure 9 (dashed line). The temperature for carbon deposition elimination was concentrated at 610 °C for $LaNiO_3$ catalyst, and its peak intensity was the highest, indicating the highest amount of carbon deposition. After the introduction of rare earth-element doping, the peak intensity of carbon deposition significantly decreases, and the elimination temperature of carbon deposition moved towards the low-temperature range [51]. The temperature for the $LaCePrNiO_3$ catalyst eliminates carbon deposition was 596 °C. This result indicates that introducing rare earth-element doping makes it easier to eliminate carbon deposition. Therefore, catalysts with low carbon deposition display good catalytic performance, as shown in Figures 6 and 8.

In addition, the SEM images of the spent catalysts of $LaNiO_3$ and $LaCePrNiO_3$ are shown in Figure S4. Obviously, $LaNiO_3$ possessed much more carbon deposition than that of $LaCePrNiO_3$, suggesting that rare earth-element doping can effectively eliminate carbon deposition, which was also verified by the above TG/DTG result.

The Raman spectra of the catalysts after the reaction is shown in Figure 10. The range of 1000 cm^{-1} to 1800 cm^{-1} is the characteristic Raman peak of carbon deposition. At 1350 cm^{-1}, it represents an amorphous carbon abbreviation (D band) with many defects [52]. And at 1598 cm^{-1}, it represents a planar C-C (sp^2) bond-stretching vibration, which is a graphitized carbon (G band) [53]. The I_D and I_G of the $LaNiO_3$ catalyst have very strong peak intensities, indicating a severe carbon deposition on the catalyst surface, with I_D: I_G = 1.51. The intensity of I_D and I_G in rare earth Ce-doped catalysts is significantly reduced, especially in Ce- and Pr-co-doped catalysts ($LaCePrNiO_3$). The intensity of its peak is weak, and I_D: I_G = 1.23. The decrease in this ratio also indicates that the elimination of carbon deposition is easier. This result is consistent with the TG and DTG analysis results mentioned above, indicating that the catalyst doped with rare earth elements has abundant oxygen vacancies, and the presence of oxygen vacancies is very effective in eliminating carbon deposition. Therefore, the catalyst doped with rare earth elements significantly enhances its ability for anti-carbon deposition.

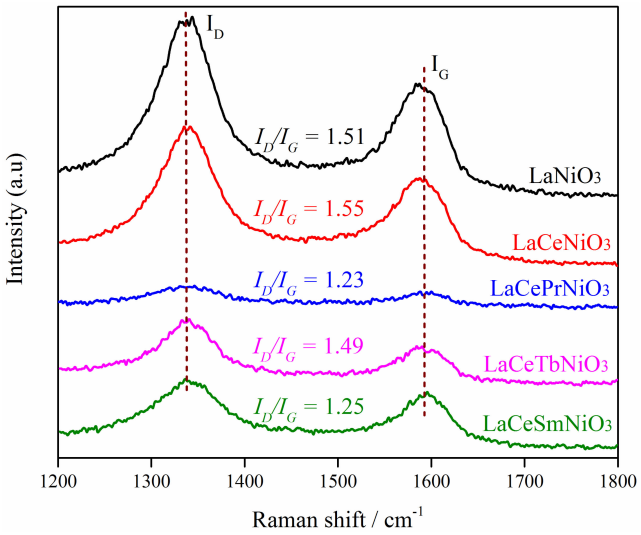

Figure 10. Raman spectra of the spent catalysts.

4. Conclusions

In a word, $LaNiO_3$ perovskite materials doped with different rare earth elements (Ce, Pr, Tb and Sm) were prepared by a sol-gel method, and perovskite-derivative-supported Ni-based catalysts were successfully synthesized by hydrogen reduction. The physical and chemical properties of the prepared catalysts were characterized using various techniques. The results showed that the calcined catalyst existed in a perovskite oxide structure, with abundant mesopores and macropores. By controlling the doping of rare earth elements (Ce,

Pr, Tb and Sm), the strength of the metal–support interaction, the size of the nickel metal particles, and the ratio of the lattice oxygen to surface oxygen on the catalyst surface can be controlled. After reduction, Ni metal nanoparticles are uniformly distributed on perovskite derivatives, and doping with rare earth elements (Ce, Pr, Tb and Sm) can effectively reduce the particle size of Ni metal. The prepared catalysts were used for hydrogen production via the steam reforming of n-dodecane. The results showed that compared to the un-doped catalyst, the activity and hydrogen production rate of the catalysts doped with rare earth elements (Ce, Pr, Tb and Sm) were significantly improved. The $LaCePrNiO_3$ catalyst has the highest activity. At 600 °C, H_2O/C = 4 and the liquid hour space velocity of 15 mL/g_{cat}·h, the conversion rate of n-dodecane reached 88%, and the hydrogen-production rate reached 6500 umol/min. After 270 min of reaction, the catalyst performance did not significantly decrease. The catalyst doped with rare earth elements significantly enhanced its ability for anti-carbon deposition, as verified by TG/DTG and Raman spectra. The reason for the high catalytic performance of $LaCePrNiO_3$ was attributed to the strong metal–support interaction between uniformly distributed Ni particles and the support, as well as the rich surface oxygen concentration of the catalyst. This work provides a simple method for preparing Ni-based catalysts with high activity and anti-carbon deposition performance for hydrogen production via the steam reforming of fuel.

Supplementary Materials: The following supporting information can be downloaded at: https://www.mdpi.com/article/10.3390/catal14030186/s1, Figure S1. The schematic diagram of experimental apparatus; Figure S2. (a) TEM images and (b) HRTEM images of $LaNiO_3$. (c) TEM images and (d) HRTEM images of $LaCePrNiO_3$, (e) The element mapping of Ce and (f) Pr of $LaCePrNiO_3$ after hydrogen reduction; Figure S3. XPS spectra of the catalysts after reduction for (a) Ce-3d, and (b) Pr-3d.; Figure S4. SEM images of spent catalysts for (a) $LaNiO_3$, and (b) $LaCePrNiO_3$. Reaction condition: 600 °C, 0.1 MPa, LHSV of $C_{12}H_{26}$ 15 mL/gcat·h, with mole ratio of H_2O:$C_{12}H_{26}$ at 24.

Author Contributions: Conceptualization, K.G. and Z.X.; methodology, K.G.; software, H.Z.; validation, K.G., H.Z. and Z.X.; formal analysis, C.Z., X.G. and H.L.; investigation, Z.X.; resources, K.G.; data curation, K.G., H.Z. and Z.X.; writing—original draft preparation, K.G., H.Z. and Z.X.; writing—review and editing, K.G., H.Z. and Z.X.; supervision, K.G.; project administration, Z.X.; funding acquisition, K.G. and Z.X. All authors have read and agreed to the published version of the manuscript.

Funding: This work was supported by the Science and Technology Project of Hebei Education Department (No. QN2023094), the Key Research and Design Program of Qinhuangdao (No. 202101A005), the Cultivation Project for Basic Research and Innovation of Yanshan University (No. 2021LGQN028), the Project for Research and Development of Metal Catalysts for Photo-thermal Decomposition of Waste Plastics to Prepare Value-added Chemicals (No. x2023322), and the Subsidy for Hebei Key Laboratory of Applied Chemistry after Operation Performance (No. 22567616H).

Data Availability Statement: The original contributions presented in the study are included in the article/Supplementary Materials, further inquiries can be directed to the corresponding author/s.

Acknowledgments: The authors gratefully acknowledge all of their co-workers for their valuable research contributions that are summarized in the present review.

Conflicts of Interest: The authors declare no conflict of interest.

References

1. Kreuer, K.D.; Paddison, S.J.; Spohr, E.; Schuster, M. Transport in proton conductors for fuel-cell applications: Simulations, elementary reactions, and phenomenology. *Chem. Rev.* **2004**, *104*, 4637–4678. [CrossRef]
2. Su, H.R.; Hu, Y.H. Progress in low-temperature solid oxide fuel cells with hydrocarbon fuels. *Chem. Eng. J.* **2020**, *402*, 126235. [CrossRef]
3. Nikolaidis, P.; Poullikkas, A. A comparative overview of hydrogen production processes. *Renew. Sustain. Energy Rev.* **2017**, *67*, 597–611. [CrossRef]
4. Park, H.G.; Han, S.Y.; Jun, K.W.; Woo, Y.; Park, M.J.; Kim, S.K. Bench-scale steam reforming of methane for hydrogen production. *Catalysts* **2019**, *9*, 615. [CrossRef]
5. Zhan, Z.; Barnett, S.A. An octane-fueled solid oxide fuel cell. *Science* **2005**, *308*, 844–848. [CrossRef]

6. Xiao, Z.; Zhang, C.; Li, P.; Wang, D.; Zhang, X.; Wang, L.; Zou, J.-J.; Li, G. Engineering oxygen vacancies on Tb-doped ceria supported Pt catalyst for hydrogen production through steam reforming of long-chain hydrocarbon fuels. *Chin. J. Chem. Eng.* **2024**, *in press*. [CrossRef]
7. Do, L.T.; Nguyen-Phu, H.; Pham, N.N.; Jeong, D.H.; Shin, E.W. Highly dispersed nickel nanoparticles on hierarchically ordered macroporous Al_2O_3 and its catalytic performance for steam reforming of 1-methyl naphthalene. *Catalysts* **2022**, *12*, 1542. [CrossRef]
8. Xie, C.; Chen, Y.S.; Engelhard, M.H.; Song, C.S. Comparative study on the sulfur tolerance and carbon resistance of supported noble metal catalysts in steam reforming of liquid hydrocarbon fuel. *ACS Catal.* **2012**, *2*, 1127–1137. [CrossRef]
9. Zheng, Q.C.; Xiao, Z.R.; Xu, J.S.; Pan, L.; Zhang, X.W.; Zou, J.J. Catalytic steam reforming and heat sink of high-energy-density fuels: Correlation of reaction behaviors with molecular structures. *Fuel* **2021**, *286*, 119371. [CrossRef]
10. Xue, Q.Q.; Li, Z.W.; Chen, M.; Wang, Y.J.; Yan, B.H.; Luo, G.S. Co-precipitation continuous synthesis of the Ni-Rh-$Ce_{0.75}Zr_{0.25}O_{2-\delta}$ catalyst in the membrane dispersion microreactor system for n-dodecane steam reforming to hydrogen. *Fuel* **2021**, *297*, 120785. [CrossRef]
11. Li, D.; Tamura, M.; Nakagawa, Y.; Tomishige, K. Metal catalysts for steam reforming of tar derived from the gasification of lignocellulosic biomass. *Bioresour. Technol.* **2015**, *178*, 53–64. [CrossRef]
12. Li, S.; Gong, J. Strategies for improving the performance and stability of Ni-based catalysts for reforming reactions. *Chem. Soc. Rev.* **2014**, *43*, 7245–7256. [CrossRef] [PubMed]
13. Shoynkhorova, T.B.; Simonov, P.A.; Potemkin, D.I.; Snytnikov, P.V.; Belyaev, V.D.; Ishchenko, A.V.; Svintsitskiy, D.A.; Sobyanin, V.A. Highly dispersed Rh-, Pt-, Ru/$Ce_{0.75}Zr_{0.25}O_{2-\delta}$ catalysts prepared by sorption-hydrolytic deposition for diesel fuel reforming to syngas. *Appl. Catal. B—Environ.* **2018**, *237*, 237–244. [CrossRef]
14. Kim, D.H.; Kang, J.S.; Lee, Y.J.; Park, N.K.; Kim, Y.C.; Hong, S.I.; Moon, D.J. Steam reforming of n-hexadecane over noble metal-modified Ni-based catalysts. *Catal. Today* **2008**, *136*, 228–234. [CrossRef]
15. Ming, Q.; Healey, T.; Allen, L.; Irving, P. Steam reforming of hydrocarbon fuels. *Catal. Today* **2002**, *77*, 51–64. [CrossRef]
16. Li, L.; Zuo, S.W.; An, P.F.; Wu, H.Y.; Hou, F.; Li, G.Z.; Liu, G.Z. Hydrogen production via steam reforming of n-dodecane over NiPt alloy catalysts. *Fuel* **2020**, *262*, 116469. [CrossRef]
17. Liu, J.; Xiao, Z.; Zhang, X. Pt and ceria promoted Ni/SBA-15 for n-dodecane steam reforming for hydrogen production. *Chem. Ind. Eng.* **2019**, *36*, 1–10.
18. Miyamoto, M.; Arakawa, M.; Oumi, Y.; Uemiya, S. Influence of metal cation doping on Ru/CeO_2/Al_2O_3 catalyst for steam reforming of desulfurized kerosene. *Int. J. Hydrogen Energy* **2015**, *40*, 2657–2662. [CrossRef]
19. Wang, T.; Liu, S.; Wang, L.; Liu, G. High-performance Rh/CeO_2 catalysts prepared by L-lysine-assisted deposition precipitation method for steam reforming of toluene. *Fuel* **2023**, *341*, 127736. [CrossRef]
20. Li, Z.W.; Li, M.; Ashok, J.; Sibudjing, K. NiCo@NiCo phyllosilicate@CeO_2 hollow core shell catalysts for steam reforming of toluene as biomass tar model compound. *Energy Convers. Manag.* **2019**, *180*, 822–830. [CrossRef]
21. Zhang, H.C.; Xiao, Z.R.; Yang, M.; Zou, J.J.; Liu, G.Z.; Zhang, X.W. Highly dispersible cerium-oxide modified Ni/SBA-15 for steam reforming of bio-mass based JP10. *Chin. J. Chem. Eng.* **2022**, *43*, 255–265. [CrossRef]
22. Tribalis, A.; Panagiotou, G.D.; Bourikas, K.; Sygellou, L.; Kennou, S.; Ladas, S.; Lycourghiotis, A.; Kordulis, C. Ni catalysts supported on modified alumina for diesel steam reforming. *Catalysts* **2016**, *6*, 11–23. [CrossRef]
23. Meloni, E.; Martino, M.; Palma, V. A short review on Ni based catalysts and related engineering issues for methane steam reforming. *Catalysts* **2020**, *10*, 352. [CrossRef]
24. Li, P.; Zhang, S.L.; Xiao, Z.R.; Zhang, H.; Ye, F.; Gu, J.M.; Wang, J.D.; Li, G.Z.; Wang, D.S. Ni-TiO_2 catalysts derived from metal-organic framework for efficient photo-thermal CO_2 methanation. *Fuel* **2024**, *357*, 129817. [CrossRef]
25. Xiao, Z.; Li, P.; Zhang, H.; Zhang, S.; Tan, X.; Ye, F.; Gu, J.; Zou, J.-j.; Wang, D. A comprehensive review on photo-thermal co-catalytic reduction of CO_2 to value-added chemicals. *Fuel* **2024**, *362*, 130906. [CrossRef]
26. Kim, H.; Lee, Y.H.; Lee, H.; Seo, J.C.; Lee, K. Effect of Mg contents on catalytic activity and coke formation of mesoporous Ni/Mg-aluminate spinel catalyst for steam methane reforming. *Catalysts* **2020**, *10*, 828. [CrossRef]
27. Xiao, Z.R.; Li, Y.T.; Hou, F.; Wu, C.; Pan, L.; Zou, J.J.; Wang, L.; Zhang, X.W.; Liu, G.Z.; Li, G.Z. Engineering oxygen vacancies and nickel dispersion on CeO_2 by Pr doping for highly stable ethanol steam reforming. *Appl. Catal. B—Environ.* **2019**, *258*, 117940. [CrossRef]
28. Xiao, Z.; Wu, C.; Wang, L.; Xu, J.; Zheng, Q.; Pan, L.; Zou, J.; Zhang, X.; Li, G. Boosting hydrogen production from steam reforming of ethanol over nickel by lanthanum doped ceria. *Appl. Catal. B—Environ.* **2021**, *286*, 119884. [CrossRef]
29. Sugisawa, M.; Takanabe, K.; Harada, M.; Kubota, J.; Domen, K. Effects of La addition to Ni/Al_2O_3 catalysts on rates and carbon deposition during steam reforming of n-dodecane. *Fuel Process. Technol.* **2011**, *92*, 21–25. [CrossRef]
30. Xiao, Z.R.; Wu, C.; Li, L.; Li, G.Z.; Liu, G.Z.; Wang, L. Pursuing complete and stable steam reforming of n-dodecane over nickel catalysts at low temperature and high LHSV. *Int. J. Hydrogen Energy* **2017**, *42*, 5606–5618. [CrossRef]
31. Ye, F.; Qian, J.; Xia, J.J.; Li, L.F.; Wang, S.J.; Zeng, Z.X.; Miao, J.; Ahamad, M.; Xiao, Z.R.; Zhang, Q.R. Effect photoelectrocatalytic degradation of pollutants over hydrophobic carbon felt loaded with Fe-doped porous carbon nitride via direct activation of molecular oxygen. *Environ. Res.* **2014**, *249*, 118497. [CrossRef]
32. Xiao, Z.R.; Li, L.; Wu, C.; Li, G.Z.; Liu, G.Z.; Wang, L. Ceria-promoted Ni–Co/Al_2O_3 catalysts for n-dodecane steam reforming. *Catal. Lett.* **2016**, *146*, 1780–1791. [CrossRef]

33. Xiao, Z.R.; Zheng, Q.C.; Zhang, X.W.; Li, L.; Wang, L.; Li, G.Z. Synthesis of Ni-Co catalysts supported on flower-like MgAl composite oxide for hydrogen production by n-dodecane steam reforming. *Chin. J. Inorg. Chem.* **2021**, *37*, 629–637.
34. Xiao, Z.R.; Ji, S.; Hou, F.; Li, Y.T.; Zhang, H.C.; Wang, L.; Zhang, X.W.; Liu, G.Z.; Zou, J.J.; Li, G.Z. n-Dodecane steam reforming catalyzed by Ni-Ce-Pr catalysts. Part 1: Catalyst preparation and Pr doping. *Catal. Today* **2018**, *316*, 78–90. [CrossRef]
35. Xiao, Z.R.; Zhang, X.W.; Hou, F.; Wu, C.; Wang, L.; Li, G.Z. Tuning metal-support interaction and oxygen vacancies of ceria supported nickel catalysts by Tb doping for n-dodecane steam reforming. *Appl. Surf. Sci.* **2020**, *503*, 144319. [CrossRef]
36. Xiao, Z.; Zhang, X.; Wang, L.; Li, G. Optimizing the preparation of Ni-Ce-Pr catalysts for efficient hydrogen production by n-dodecane steam reforming. *Int. J. Energy Res.* **2019**, *44*, 1828–1842. [CrossRef]
37. Oemar, U.; Ang, P.S.; Hidajat, K.; Kawi, S. Promotional effect of Fe on perovskite $LaNi_xFe_{1-x}O_3$ catalyst for hydrogen production via steam reforming of toluene. *Int. J. Hydrogen Energy* **2013**, *38*, 5525–5534. [CrossRef]
38. Chen, G.K.; Shen, Q.W.; Zhang, X.; Cai, Z.W.; Shao, Z.C.; Li, S.; Yang, G.G. Methanol steam reforming over $La_{1-x}Sr_xCeO_{3-\delta}$ catalysts for hydrogen production: Optimization of operating parameters. *Catalysts* **2023**, *13*, 248. [CrossRef]
39. Wang, Y.; Qian, S.; Chen, Y.; Yan, B.; Cheng, Y. Effect of the calcination temperature of $LaNiO_3$ on the structural properties and reaction performance of catalysts in the steam reforming of methane. *Catalysts* **2023**, *13*, 356. [CrossRef]
40. Das, S.; Bhattar, S.; Liu, L.N.; Wang, Z.G.; Xi, S.B.; Spivey, J.J.; Kawi, S. Effect of partial Fe substitution in $La_{0.9}Sr_{0.1}NiO_3$ perovskite-derived catalysts on the reaction mechanism of methane dry reforming. *ACS Catal.* **2020**, *10*, 12466–12486. [CrossRef]
41. Pereñiguez, R.; Gonzalez-delaCruz, V.M.; Caballero, A.; Holgado, J.P. $LaNiO_3$ as a precursor of Ni/La_2O_3 for CO_2 reforming of CH_4: Effect of the presence of an amorphous NiO phase. *Appl. Catal. B—Environ.* **2012**, *123–124*, 324–332. [CrossRef]
42. Yu, J.B.; Muhetaer, A.; Gao, X.W.; Zhang, Z.Z.; Yang, Y.Y.; Li, Q.; Chen, L.X.; Liu, H.C.; Xu, D.S. Highly active hydrogen-rich photothermal reverse water gas shift reaction on $Ni/LaInO_3$ perovskite catalysts with near-unity selectivity. *Angew. Chem. Int. Ed.* **2023**, *62*, e202303135. [CrossRef]
43. Wu, G.W.; Li, S.R.; Zhang, C.X.; Wang, T.; Gong, J.L. Glycerol steam reforming over perovskite-derived nickel-based catalysts. *Appl. Catal. B—Environ.* **2014**, *144*, 277–285. [CrossRef]
44. De Lima, S.M.; da Silva, A.M.; da Costa, L.O.O.; Assaf, J.M.; Jacobs, G.; Davis, B.H.; Mattos, L.V.; Noronha, F.B. Evaluation of the performance of Ni/La_2O_3 catalyst prepared from $LaNiO_3$ perovskite-type oxides for the production of hydrogen through steam reforming and oxidative steam reforming of ethanol. *Appl. Catal. A* **2010**, *377*, 181–190. [CrossRef]
45. Liu, H.; Yu, J. Catalytic performance of $Cu\text{-}Ni/La_{0.75}Sr_{0.25}Cr_{0.5}Mn_{0.5}O_{3-\delta}$ for dry methane reforming. *Int. J. Energy Res.* **2022**, *46*, 10522–10534. [CrossRef]
46. Bussi, J.; Musso, M.; Quevedo, A.; Faccio, R.; Romero, M. Structural and catalytic stability assessment of Ni-La-Sn ternary mixed oxides for hydrogen production by steam reforming of ethanol. *Catal. Today* **2017**, *296*, 154–162. [CrossRef]
47. Kim, T.; Song, K.H.; Yoon, H.; Chung, J.S. Steam reforming of n-dodecane over $K_2Ti_2O_5$-added Ni-alumina and Ni-zirconia (YSZ) catalysts. *Int. J. Hydrogen Energy* **2016**, *41*, 17922–17932. [CrossRef]
48. Li, D.L.; Koike, M.; Chen, J.H.; Nakagawa, Y.; Tomishige, K. Preparation of Ni-Cu/Mg/Al catalysts from hydrotalcite-like compounds for hydrogen production by steam reforming of biomass tar. *Int. J. Hydrogen Energy* **2014**, *39*, 10959–10970. [CrossRef]
49. Jing, J.Y.; Wei, Z.H.; Zhang, Y.B.; Bai, H.C.; Li, W.Y. Carbon dioxide reforming of methane over MgO-promoted Ni/SiO_2 catalysts with tunable Ni particle size. *Catal. Today* **2020**, *356*, 589–596. [CrossRef]
50. Xiao, Z.R.; Li, P.; Zhang, S.L.; Gu, J.M.; Wang, D.S. Effects of metal-support interactions and interfaces on catalytic performance over M_2O_3- (M = La, Al-) supported Ni catalysts. *Int. J. Energy Res.* **2023**, *2023*, 6504914. [CrossRef]
51. Li, D.; Zeng, L.; Li, X.Y.; Wang, X.; Ma, H.Y.; Assabumrungrat, S.; Gong, J.L. Ceria-promoted Ni/SBA-15 catalysts for ethanol steam reforming with enhanced activity and resistance to deactivation. *Appl. Catal. B—Environ.* **2015**, *176*, 532–541. [CrossRef]
52. Chen, M.Q.; Wang, Y.S.; Yang, Z.L.; Liang, T.; Liu, S.M.; Zhou, Z.S.; Li, X.J. Effect of Mg-modified mesoporous Ni/Attapulgite catalysts on catalytic performance and resistance to carbon deposition for ethanol steam reforming. *Fuel* **2018**, *220*, 32–46. [CrossRef]
53. Xue, Q.Q.; Li, Z.W.; Yi, H.L.; Jiang, Z.; Yan, B.H.; Wang, Y.J.; Luo, G.S. Controlling sintering and carbon deposition with post-coated MgO confined group VIII metal-based catalysts towards durable high-temperature steam reforming. *Appl. Catal. B—Environ.* **2022**, *318*, 121874. [CrossRef]